

Field analysis of a dielectric-loaded rectangular waveguide accelerating structure

Liling Xiao, Wei Gai, and Xiang Sun

High Energy Physics Division, Argonne National Laboratory, Argonne, Illinois 60439

(Received 23 March 2001; revised manuscript received 2 July 2001; published 19 December 2001)

Recently, there has been some interest in planar or rectangular dielectric accelerating structures for future high-gradient linear accelerators. In this paper, we present a detailed analysis of the modes of a dielectric-loaded rectangular waveguide accelerating structure based on a circuit model approximation and mode matching method. In general, the acceleration field in a synchronous acceleration mode is nonuniform in the two transverse dimensions. We show, however, that by using a series of rectangular structures successively rotated by 90° , the net accelerating force can be made almost uniform. Characteristic parameters such as R/Q , group velocity, and attenuation constant for X - and W -band accelerators are calculated. The longitudinal wakefields experienced by a relativistic charged particle beam in these structures are also presented. These analytical results are also compared with numerical calculations using the MAFIA code suite demonstrating the validity of our analytic approach.

DOI: 10.1103/PhysRevE.65.016505

PACS number(s): 41.75.Lx, 29.17.+w, 42.82.Et, 84.40.-x

I. INTRODUCTION

The possible applications of millimeter-wave dielectric waveguide accelerating structures to high-energy accelerator have received much attention [1–6]. This class of accelerating structures can produce a high accelerating gradient and can easily be fabricated. Dielectric-loaded structures have also found application in a variety of waveguide components such as phase shifters, matching transformers, and quarter-wave plates. Any dielectric slow wave structure can support traveling-wave luminal accelerating modes, but so far studies of such structures have mainly concentrated on cylindrical structures operating at X band [6]. In order to avoid breakdown of the structure at higher accelerating fields, it is desirable to use accelerating structures operating at higher frequencies [7], such as at W band. On the other hand, while higher-frequency cylindrical structures would yield higher accelerating fields and shunt impedances, the stored energy per unit length is very low so that the accelerated beam current is limited. Therefore, simply scaling cylindrical geometry structures to higher frequencies will not lead to a higher luminosity accelerator. It also becomes increasingly difficult to fabricate and tune a high-frequency dielectric-lined cylindrical structure.

A class of structures, which overcomes these difficulties, uses the slab geometry shown in Fig. 1. Some advantages of the rectangular slab geometry over cylindrical dielectric structures at high frequencies are given.

Tuning: The structure can be easily tuned to correct frequency error by adjusting the metallic side walls that are free of dielectric.

Stored energy: For a given frequency and accelerating gradient the rectangular structure can store more energy than a cylindrical dielectric structure thus reducing beam loading.

Focusing: The accelerating field is not uniform across the transverse dimensions, so unlike the TM accelerating modes in a cylindrical structure the transverse forces on a relativistic beam do not cancel, but provide a focusing force that acts

on the beam like an rf quadrupole while the beam is accelerated.

It is necessary to perform a detailed three-dimensional (3D) field analysis for the rectangular structure. There have been some efforts to study slab-symmetric dielectric-loaded accelerating structures at very high frequencies [4,5]. In these cases, the field calculations for slab geometry concentrated on a two-dimensional analysis that assumes the width of the structure is infinite. The problem associated with the 2D analysis is that it does not accurately describe the field profiles in transverse directions to the beam axis. In this paper we calculate 3D field distributions for a rectangular partially filled dielectric waveguide, and we present an exact solution for all the field components in terms of LSM (longitudinal section magnetic) and LSE (longitudinal section electric) modes using a mode matching method. This analysis provides a basis for studying the properties of this structure as an accelerator. We also present a wakefield calculation using the field analysis results. We calculate the shunt impedance R and quality factor Q for each mode, which in turn provides the Green functions for the wakefield excitations.

II. FIELD ANALYTICAL APPROACH

The normal modes in dielectric-loaded guides are not, in general, either pure E or H modes, but rather combinations of those modes. An exception is the case of H_{0n} modes where the electric field is parallel to the dielectric slab and there is no variation of the fields along the vacuum-dielectric interface. In this case, another set of modes can be adopted for dielectric-loaded guides that have no H or E components normal to the interface. These modes have been designated LSM and LSE modes [8]. This corresponds to assuming the transverse direction to the interface normal vector to be the direction of propagation.

The cross section of a dielectric-loaded rectangular guide can be divided into three homogeneous subregions (vacuum and the two dielectric slabs) as shown in Fig. 1. The general

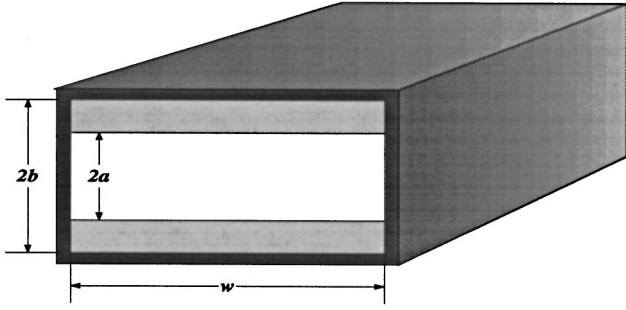


FIG. 1. Dielectric-loaded rectangular guide.

structure considered here is limited to the case of two H -plane slabs placed symmetrically. We also only analyze these modes with the longitudinal electric components at the central point since any other modes will not couple to the beam. It implies that the central plane in the y - z view is a magnetic wall, so that only a half section with two subregions is needed for the analysis [Fig. 2(a)]. In this paper, the transverse resonance technique (TRT) is applied to study the propagation properties in the structure [9]. In each region, the fields for LSM/LSE modes derive from the electric/magnetic Hertzian potential and satisfy the boundary conditions at dielectric and vacuum interfaces.

A. Dispersion relations

The transverse equivalent circuit can be established as shown in Fig. 2(b), and in fact, it holds for both LSM and LSE modes. Two transmission line sections correspond to the LSM_{mn} or LSE_{mn} mode in the two regions $0 < y < a$ and $a < y < b$. The lateral walls at $y=0$ and b correspond to open and short circuits, respectively. The field continuity at the dielectric-vacuum interface implies the continuity of both the voltage and current, and thus is represented by the direct connection of the two equivalent transmission line sections.

For nonzero voltages and currents in the transverse equivalent circuit, the resonance condition must be satisfied.

$$-Z_{0mn}^{(0)} \cot(k_{ymn}^{(0)} a) + Z_{0mn}^{(1)} \tan[k_{ymn}^{(1)} (b-a)] = 0, \quad (1)$$

where the values of the characteristic impedances will depend on the type of mode being considered,

$$Z_{0mn}^{(0)} = \frac{k_{ymn}^{(0)}}{\omega \epsilon_0}, \quad Z_{0mn}^{(1)} = \frac{k_{ymn}^{(1)}}{\omega \epsilon_0 \epsilon_r} \quad (\text{LSM}_{mn}), \quad (2a)$$

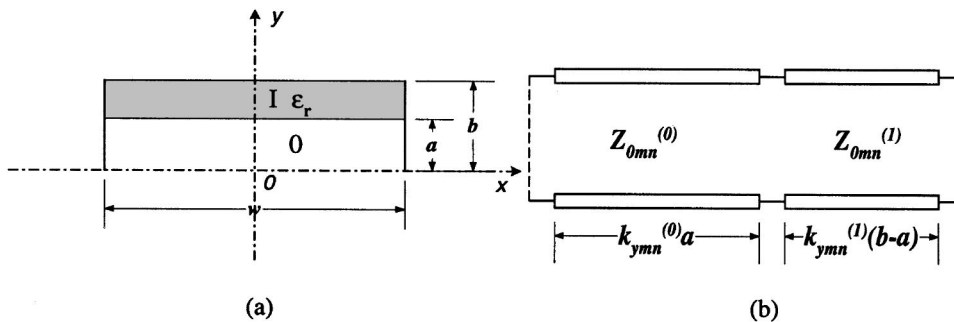


FIG. 2. The half cross section of the rectangular structure (a) and its transverse equivalent circuit (b).

$$Z_{0mn}^{(0)} = \frac{\omega \mu_0}{k_{ymn}^{(0)}}, \quad Z_{0mn}^{(1)} = \frac{\omega \mu_0}{k_{ymn}^{(1)}} \quad (\text{LSE}_{mn}). \quad (2b)$$

The transverse propagation constants can be expressed in terms of the longitudinal propagation constant β_{mn} using the following conditions:

$$k_{ymn}^{(0)2} = k^2 - \left(\frac{m\pi}{w}\right)^2 - \beta_{mn}^2, \quad k_{ymn}^{(1)2} = \epsilon_r k^2 - \left(\frac{m\pi}{w}\right)^2 - \beta_{mn}^2, \quad (3)$$

where $k = 2\pi f/c$ is the propagation constant in free space.

Inserting Eqs. (3) and (2a) or Eq. (2b) into Eq. (1), we can obtain the dispersion relations of the LSM_{mn} or LSE_{mn} modes in the dielectric-loaded rectangular guide,

$$k_{ymn}^{(1)} \sin[k_{ymn}^{(1)} (b-a)] \sin k_{ymn}^{(0)} a - \epsilon_r k_{ymn}^{(0)} \cos(k_{ymn}^{(0)} a) \cos[k_{ymn}^{(1)} (b-a)] = 0 \quad (\text{LSM}_{mn}), \quad (4a)$$

$$k_{ymn}^{(0)} \sin[k_{ymn}^{(1)} (b-a)] \sin k_{ymn}^{(0)} a - k_{ymn}^{(1)} \cos(k_{ymn}^{(0)} a) \times \cos[k_{ymn}^{(1)} (b-a)] = 0 \quad (\text{LSE}_{mn}). \quad (4b)$$

This is a transcendental equation of the general form of a complex function of β_{mn} and f . For the inhomogeneous guide considered here, the dispersion relation must be solved at each frequency. Again an infinite number of discrete solutions exist. We will only solve the first solution for each m index at each frequency, corresponding to the LSM_{m1} or LSE_{m1} mode.

B. Field components

1. LSM_{mn} modes

In each region, the fields for the LSM_{mn} derive from an electric-type Hertzian potential. Using the boundary conditions at the perfectly conducting guide walls ($x = \pm w/2$, $y = b$) and the boundary condition at the magnetic wall ($y = 0$), the potential function ψ_e is

$$\psi_{emn} = \begin{cases} A_{mn} \sin \frac{m\pi}{w} \left(x + \frac{w}{2} \right) \sin k_{ymn}^{(0)} y e^{-j\beta_{mn}z}, & 0 < y < a, \\ B_{mn} \sin \frac{m\pi}{w} \left(x + \frac{w}{2} \right) \cos k_{ymn}^{(1)} (b-y) e^{-j\beta_{mn}z}, & a < y < b. \end{cases} \quad (5)$$

The field components for the LSM_{mn} are given by

$$\begin{aligned} E_{xmn} &= \begin{cases} A_{mn} \frac{m\pi}{w} k_{ymn}^{(0)} \cos \frac{m\pi}{w} \left(x + \frac{w}{2} \right) \cos k_{ymn}^{(0)} y, & 0 < y < a, \\ B_{mn} \frac{m\pi}{w} k_{ymn}^{(1)} \cos \frac{m\pi}{w} \left(x + \frac{w}{2} \right) \sin k_{ymn}^{(1)} (b-y), & a < y < b, \end{cases} \\ E_{ymn} &= \begin{cases} A_{mn} k_{cmn}^2 \sin \frac{m\pi}{w} \left(x + \frac{w}{2} \right) \sin k_{ymn}^{(0)} y, & 0 < y < a, \\ B_{mn} k_{cmn}^2 \sin \frac{m\pi}{w} \left(x + \frac{w}{2} \right) \cos k_{ymn}^{(1)} (b-y), & a < y < b, \end{cases} \\ E_{zmn} &= \begin{cases} A_{mn} (-j\beta_{mn}) k_{ymn}^{(0)} \sin \frac{m\pi}{w} \left(x + \frac{w}{2} \right) \cos k_{ymn}^{(0)} y, & 0 < y < a, \\ B_{mn} (-j\beta_{mn}) k_{ymn}^{(1)} \sin \frac{m\pi}{w} \left(x + \frac{w}{2} \right) \sin k_{ymn}^{(1)} (b-y), & a < y < b, \end{cases} \\ H_{xmn} &= \begin{cases} -A_{mn} \omega \varepsilon_0 \beta_{mn} \sin \frac{m\pi}{w} \left(x + \frac{w}{2} \right) \sin k_{ymn}^{(0)} y, & 0 < y < a, \\ -B_{mn} \omega \varepsilon_0 \varepsilon_r \beta_{mn} \sin \frac{m\pi}{w} \left(x + \frac{w}{2} \right) \cos k_{ymn}^{(1)} (b-y), & a < y < b, \end{cases} \\ H_{ymn} &= 0 \\ H_{zmn} &= \begin{cases} A_{mn} (j\omega \varepsilon_0) \frac{m\pi}{w} \cos \frac{m\pi}{w} \left(x + \frac{w}{2} \right) \sin k_{ymn}^{(0)} y, & 0 < y < a, \\ B_{mn} (j\omega \varepsilon_0 \varepsilon_r) \frac{m\pi}{w} \cos \frac{m\pi}{w} \left(x + \frac{w}{2} \right) \cos k_{ymn}^{(1)} (b-y), & a < y < b, \end{cases} \end{aligned} \quad (6)$$

where $k_{cmn}^2 = (m\pi/w)^2 + \beta_{mn}^2$. Note that the z dependence $\exp(-j\beta_{mn}z)$ has been omitted in these expressions for simplicity.

At the interface between the region 0 and I, the tangential electric and magnetic field components must all be continuous so the following conditions are imposed on the solution given by Eq. (6)

$$A_{mn} K_{ymn}^{(0)} \cos k_{ymn}^{(0)} a = B_{mn} k_{ymn}^{(1)} \sin k_{ymn}^{(1)} (b-a), \quad (7a)$$

$$A_{mn} \sin k_{ymn}^{(0)} a = B_{mn} \varepsilon_r \cos k_{ymn}^{(1)} (b-a). \quad (7b)$$

Dividing Eq. (7a) by Eq. (7b) yields the dispersion relation, which is the same as Eq. (4a). From Eq. (7), the coefficient ratio can be found, and, when substituted into Eq. (6), completes the solution.

2. LSE_{mn} modes

The derivation for the LSE_{mn} modes follows the same lines as the one for the LSM_{mn} modes. A magnetic-type potential function ψ_h is

$$\psi_{hmn} = \begin{cases} C_{mn} \frac{1}{j\omega\mu_0} \cos \frac{m\pi}{w} \left(x + \frac{w}{2} \right) \cos k_{ymn}^{(0)} y e^{-j\beta_{mn}z}, & 0 < y < a, \\ D_{mn} \frac{1}{j\omega\mu_0} \cos \frac{m\pi}{w} \left(x + \frac{w}{2} \right) \sin k_{ymn}^{(1)} (b-y) e^{-j\beta_{mn}z}, & a < y < b. \end{cases} \quad (8)$$

The corresponding field components are derived from Eq. (8), (again omitting the z dependence for brevity),

$$\begin{aligned}
E_{xmn} &= \begin{cases} C_{mn}(-j\beta_{mn})\cos\frac{m\pi}{w}\left(x+\frac{w}{2}\right)\cos k_{ymn}^{(0)}y, & 0 < y < a, \\ D_{mn}(-j\beta_{mn})\cos\frac{m\pi}{w}\left(x+\frac{w}{2}\right)\sin k_{ymn}^{(1)}(b-y), & a < y < b, \end{cases} \\
E_{zmn} &= 0 \\
E_{zmn} &= \begin{cases} C_{mn}\frac{m\pi}{w}\sin\frac{m\pi}{w}\left(x+\frac{w}{2}\right)\cos k_{ymn}^{(0)}y, & 0 < y < a, \\ D_{mn}\frac{m\pi}{w}\sin\frac{m\pi}{w}\left(x+\frac{w}{2}\right)\sin k_{ymn}^{(1)}(b-y), & a < y < b, \end{cases} \\
H_{xmn} &= \begin{cases} C_{mn}\frac{k_{ymn}^{(0)}}{j\omega\mu_0}\frac{m\pi}{w}\sin\frac{m\pi}{w}\left(x+\frac{w}{2}\right)\sin k_{ymn}^{(0)}y, & 0 < y < a, \\ D_{mn}\frac{k_{ymn}^{(1)}}{j\omega\mu_0}\frac{m\pi}{w}\sin\frac{m\pi}{w}\left(x+\frac{w}{2}\right)\cos k_{ymn}^{(1)}(b-y), & a < y < b, \end{cases} \quad (9) \\
H_{ymn} &= \begin{cases} C_{mn}\frac{k_{cmn}^2}{j\omega\mu_0}\cos\frac{m\pi}{w}\left(x+\frac{w}{2}\right)\cos k_{ymn}^{(0)}y, & 0 < y < a, \\ D_{mn}\frac{k_{cmn}^2}{j\omega\mu_0}\cos\frac{m\pi}{w}\left(x+\frac{w}{2}\right)\sin k_{ymn}^{(1)}(b-y), & a < y < b, \end{cases} \\
H_{zmn} &= \begin{cases} C_{mn}\frac{\beta_{mn}k_{ymn}^{(0)}}{\omega\mu_0}\cos\frac{m\pi}{w}\left(x+\frac{w}{2}\right)\sin k_{ymn}^{(0)}y, & 0 < y < a, \\ D_{mn}\frac{\beta_{mn}k_{ymn}^{(1)}}{\omega\mu_0}\cos\frac{m\pi}{w}\left(x+\frac{w}{2}\right)\cos k_{ymn}^{(1)}(b-y), & a < y < b. \end{cases}
\end{aligned}$$

Similarly, the coefficient ratio and the dispersion relation can be obtained using the field continuity at $y=a$.

III. GENERAL ACCELERATION PROPERTIES OF THE LSM₁₁ MODE

In general, the relative advantages of accelerating structures can be understood with reference to figures of merit such as the ratio of the peak surface electric field to the axial acceleration field E_s/E_0 , the group velocity v_g , the attenuation constant α , and R/Q that measures the efficiency of acceleration in term of the given stored energy, etc. The definitions of these parameters will be briefly discussed and quantified here. In this section, only the results pertaining to the LSM₁₁ mode are given, because the LSM₁₁ mode is the lowest luminal mode in our considered structures, and its longitudinal electric field is distributed symmetrically in both x and y . All other higher-order mode properties can be obtained using similar methods, although they are only relevant to the wakefield calculations shown in Sec. V.

A. The ratio of surface field E_s to accelerating field E_z

The axial electrical field E_z in the vacuum region is

$$E_z = E_0 \sin\frac{\pi}{w}\left(x+\frac{w}{2}\right)\cos k_y^{(0)}y \cos\beta z. \quad (10)$$

The ratio of surface field E_s to accelerating field E_0 is

$$\begin{aligned}
\left|\frac{E_s}{E_0}\right| &= \left|\frac{E_y(0,b)}{E_z(0,0)}\right| = \left|\frac{\left(\frac{\pi}{w}\right)^2 + \beta^2}{k_y\beta} \sin k_y a\right| \\
&= \frac{\left(\frac{\pi}{w}\right)^2 + \beta^2}{\frac{\pi}{w}\beta} \left|\sin\left(\frac{\pi}{w}a\right)\right|. \quad (11)
\end{aligned}$$

It is desirable to have this ratio as small as possible since the surface field contributes nothing to accelerating the beam but is responsible for breakdown of the structure.

B. The group velocity v_g , power flow P , and stored energy U

The relationship between the group velocity v_g , power flow P , and stored energy U in this type of structure is the same as for a standard waveguide [10].

$$v_g = \frac{P}{U},$$

$$P = \frac{1}{2} \iint E_y H_x dx dy, \quad (12)$$

$$\begin{aligned}
U &= \frac{1}{2L} \iiint [\epsilon_0 \epsilon_r(y)(E_x^2 + E_y^2 + E_z^2) \\
&\quad + \mu_0(H_x^2 + H_z^2)] dx dy dz,
\end{aligned}$$

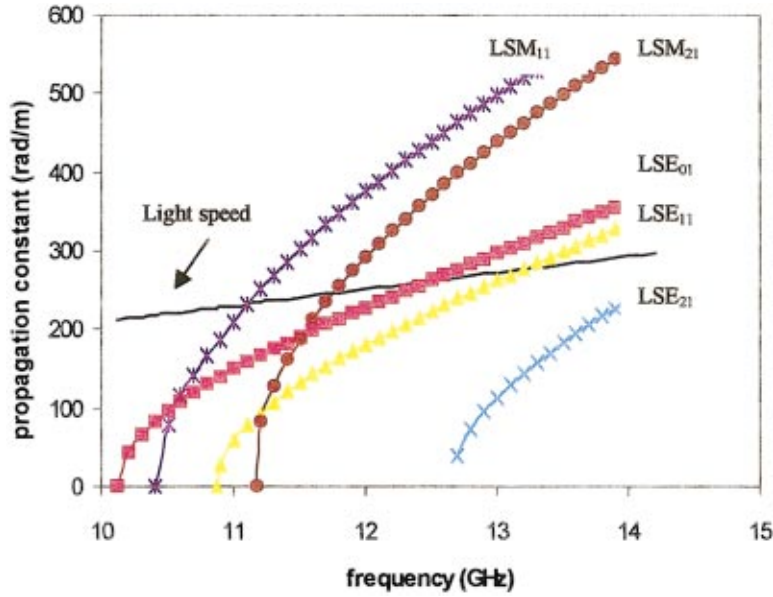


FIG. 3. (Color) Dispersion curves of an X-band dielectric-loaded rectangular guide ($a = 3$ mm, $b = 5$ mm, $w = 23$ mm, and $\epsilon_r = 10$).

where P is the power flow over the half section under consideration and U is the stored energy per unit length in the half structure.

C. The quality factor Q (ignoring dielectric losses) and the attenuation constant α

In general, the rf losses in this class of structures are from ohmic losses in the walls. Dielectric losses are much lower because high- Q dielectric materials, now commonly available, can be used. Thus, for a given field distribution, and with the calculated stored energy and power losses on the walls, we have the system Q as

$$Q = \frac{\omega U}{P_{\text{loss}}},$$

$$P_{\text{loss}} = R_s \int \int |\vec{H}|^2 ds, \quad (13)$$

$$R_s = \frac{1}{\delta_{\text{skin}} \sigma} \quad \text{and} \quad \delta_{\text{skin}} = \sqrt{\frac{2}{\mu_0 \sigma \omega}},$$

where σ is the conductivity of the metal wall.

The attenuation constant α is given by

$$\alpha = \frac{\omega}{2Qv_g} = \frac{P_{\text{loss}}}{2P}. \quad (14)$$

D. The normalized shunt impedance R/Q

For a linear accelerator system, it is common and very important for comparison of different types of accelerating structures to calculate a normalized impedance R/Q , which is a measure of overall effectiveness of the acceleration structure.

$$\frac{R}{Q} = \frac{E_0^2 v_g}{\omega P}, \quad (15)$$

where E_0 is the maximum accelerating field on the z axis.

IV. FIELD PROPERTIES DISCUSSION AND NUMERICAL RESULTS

Figure 3 shows the dispersion curves of the lower LSM_{m1} and LSE_{m1} modes for a structure with $a = 3$ mm, $b = 5$ mm, $w = 23$ mm, and $\epsilon_r = 10$. LSM_{11} and LSE_{01} modes are the lowest symmetrical LSM and LSE modes, respectively, and the LSM_{11} mode is the lowest symmetrical synchronous mode in this structure with excitation frequency of 11.17 GHz (X band).

Now let us examine the field distributions of a LSM_{11} mode synchronous with and acting upon an ultrarelativistic electron ($\beta = 2\pi f/c = k$). In vacuum (region 0), $k_x^2 = -k_y^2 = (\pi/w)^2$; k_y is imaginary and of equal amplitude with k_x . (This phenomenon had been investigated in slab-symmetric dielectric structures [4], but in the limit $w \rightarrow \infty$ so that $k_x^2 = -k_y^2 = 0$). This transverse dependence of the fields will result in focusing in the x direction and defocusing in y ; the dielectric-loaded rectangular guide accelerating structure can thus be thought of as a quadrupole in terms of its focusing properties. Figure 4 gives the normalized longitudinal electric field distributions of the LSM_{11} synchronous mode as a function of x and y using the field analysis method.

When the x dimension tends to infinity, the fields in the dielectric-loaded rectangular accelerating structure approach those of the planar dielectric guide described in Refs. [4,5]. In this limit the LSM_{11} mode will only have three components (E_x , E_z , and H_y) and be the same as the accelerating mode in a planar dielectric structure [5].

As one can see, this field is not independent of x and y . This would result in nonuniform energy gain of charged particles passing through different locations. This is different than a conventional cylindrical structure. Furthermore, this nonuniform E_z also means that there are transverse forces F_x and F_y exerted on a charged particle with charge e passing through the structure. These forces are given by

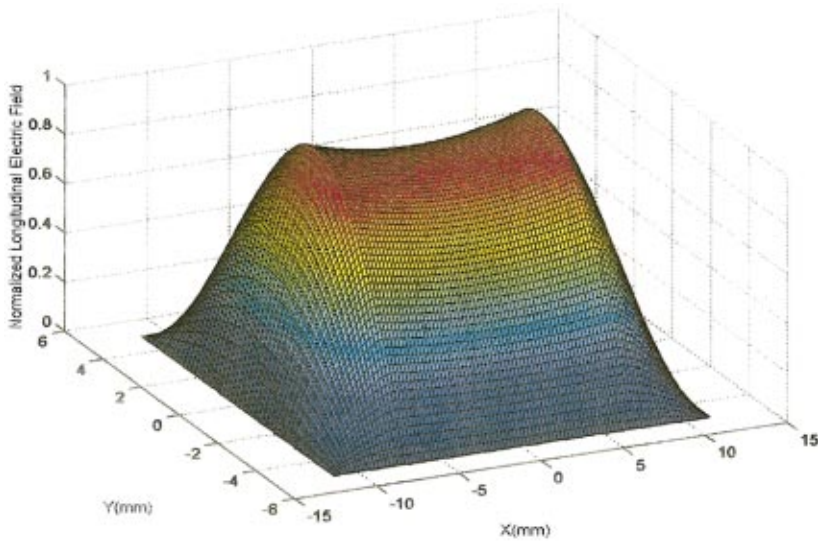


FIG. 4. (Color) The normalized longitudinal electric field distribution at transverse section using the field analysis method in Sec. II ($a=3$ mm, $b=5$ mm, $w=23$ mm, and $\epsilon_r=10$).

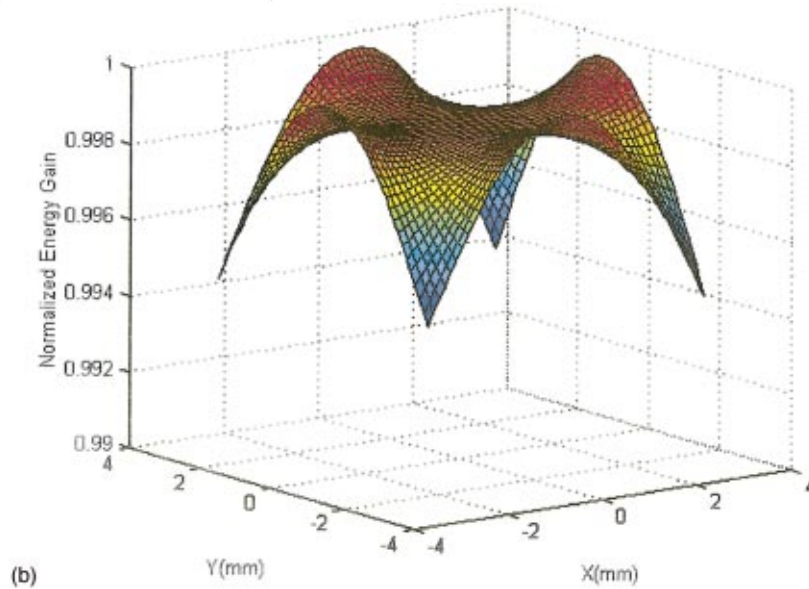
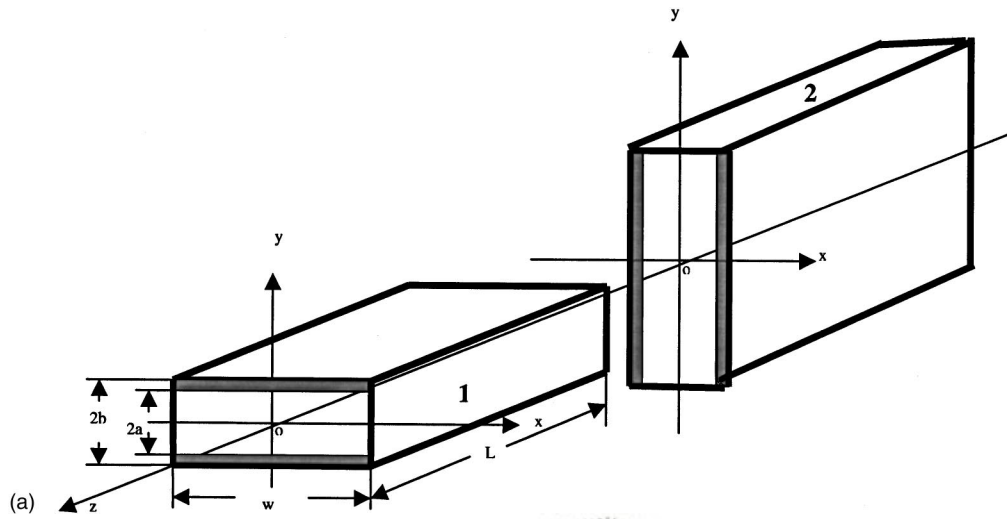


FIG. 5. (Color) Two orthogonal identical accelerating structures (a) and the net normalized energy gain experienced by a particle in the region $-a < x < a$ and $-a < y < a$ (b). In the central area, the net energy gain experienced by the beam after passing through the two orthogonal identical accelerating structures is uniform ($a=3$ mm, $b=5$ mm, $w=23$ mm, and $\epsilon_r=10$).

$$F_x = eE_0 \frac{\pi}{w} \cos \frac{\pi}{w} \left(x + \frac{w}{2} \right) \cos k_y^{(0)} y \sin \beta z,$$

$$F_y = eE_0 (-k_y^{(0)}) \sin \frac{\pi}{w} \left(x + \frac{w}{2} \right) \sin k_y^{(0)} y \sin \beta z. \quad (16)$$

Since $-k_y^{(0)} = j(\pi/w)$, and assuming that x and y are very small, we have $F_x = -F_y$. This can be viewed as a focusing force on the particle from a quadrupole field and with focusing strength $\propto 1/w$. An array of these structures rotated alternately by 90° will provide a net force continuously analogous to a simple focusing and defocusing (FODO) lattice. The integrated acceleration force in the center area will be very close to uniform, just as in a conventional cylindrical iris-loaded accelerating structure.

To simplify the discussion, let us first consider two identical structures (1 and 2) rotated by 90° . These two structures are not electrically coupled as shown in Fig. 5(a). Each accelerator section is powered independently with the same external rf source. Next we calculate the net energy gain after passing through structures 1 and 2. The acceleration fields in structures 1 and 2 are the same LSM₁₁ mode operating at the same frequency and amplitude. Due to the orthogonality of the two structures, the field distributions will correspond to $H_y = 0$ in structure 1 and $H_x = 0$ in structure 2 as we discussed in Sec. II. We will use the notation LSM₁₁^(y) and LSM₁₁^(x) to indicate the accelerating modes in structures 1 and 2. Their longitudinal electric field components are given in Eq. (17).

$$E_z^1 = \begin{cases} A_{11}(-j\beta_{11})k_{y11}^{(0),1} \sin \frac{\pi}{w} \left(x + \frac{w}{2} \right) \cos k_{y11}^{(0),1} y e^{j2\pi fz}, & |x| < w/2, \quad |y| < a, \\ B_{11}(-j\beta_{11})k_{y11}^{(1),1} \sin \frac{\pi}{w} \left(x + \frac{w}{2} \right) \sin k_{y11}^{(1),1} (b-y) e^{j2\pi fz}, & |x| < w/2, \quad a < |y| < b, \end{cases} \quad (\text{LSM}_{11}^{(y)})$$

$$E_z^2 = \begin{cases} A_{11}(-j\beta_{11})k_{x11}^{(0),2} \sin \frac{\pi}{w} \left(y + \frac{w}{2} \right) \cos k_{x11}^{(0),2} x e^{j2\pi fz}, & |y| < w/2, \quad |x| < a, \\ B_{11}(-j\beta_{11})k_{x11}^{(1),2} \sin \frac{\pi}{w} \left(y + \frac{w}{2} \right) \sin k_{x11}^{(1),2} (b-x) e^{j2\pi fz}, & |y| < w/2, \quad a < |x| < b, \end{cases} \quad (\text{LSM}_{11}^{(x)}) \quad (17)$$

where $\beta_{11} = 2\pi f/c = k$, and $k_{y11}^{(0),1} = k_{x11}^{(0),2} = j(\pi/w)$.

This means that in vacuum regions of structures 1 and 2, the $k_{y11}^{(0),1}$ and $k_{x11}^{(0),2}$ are imaginary and of equal amplitude with π/w . The longitudinal electric field components in vacuum regions can be expressed as

$$E_z^1 = jA_{11}(-j\beta_{11}) \frac{\pi}{w} \cos \frac{\pi}{w} x \cosh \frac{\pi}{w} y e^{j2\pi fz},$$

$$|x| < w/2, \quad |y| < a,$$

$$E_z^2 = jA_{11}(-j\beta_{11}) \frac{\pi}{w} \cos \frac{\pi}{w} y \cosh \frac{\pi}{w} x e^{j2\pi fz},$$

$$|x| < a, \quad |y| < w/2. \quad (18)$$

After passing through structures 1 and 2, the net energy gain experienced by a particle in the region $-a < x < a$ and $-a < y < a$ is

$$W_z(x,y) = eE_z(x,y)L$$

$$= eL \left[jA_{11}(-j\beta_{11}) \frac{\pi}{w} \cos \frac{\pi}{w} x \cosh \frac{\pi}{w} y e^{j2\pi fL} \right. \\ \left. + jA_{11}(-j\beta_{11}) \frac{\pi}{w} \cos \frac{\pi}{w} y \cosh \frac{\pi}{w} x e^{j2\pi fL} \right], \quad (19)$$

$$= eLA_{11}\beta_{11} \frac{\pi}{w} e^{j2\pi fL} \left(\cos \frac{\pi}{w} x \cosh \frac{\pi}{w} y \right. \\ \left. + \cos \frac{\pi}{w} y \cosh \frac{\pi}{w} x \right) \\ = eLA_{11}\beta_{11} \frac{\pi}{w} e^{j2\pi fL} f(x,y).$$

Equation (19) shows that the integrated accelerating field is nearly constant in the region of interest in both x and y views. Figure 5(b) gives the normalized $W_z(x,y)$ distribu-

TABLE I. Accelerating parameters for the example X-band and W-band structures.

Size	f (GHz)	β (rad/m)	Q	E_s/E_0	V_g/c	R/Q (k Ω /m)	α
X band (analytic)	11.17	234.0	3566	0.5	0.13	12.6	0.26
X band (MAFIA)	11.17	235.4	3630				
W band (analytic)	92.81	1945	1281	0.4	0.12	106	6.16
W band (Ref. [5])	91.41		1400	0.6	0.1		6.8

tions as a function of x and y calculated from Eq. (19). One can show that $f(x,y)$ is constant to fourth order in small x and y offsets. In the case studied here, the maximal and minimal net energy gain for particles at different transverse positions differ by $<0.6\%$. It could be reduced further if the beam is confined to a smaller transverse regions as would be the case in a conventional accelerating structure.

Table I lists the general parameters of X - and W -band dielectric-loaded rectangular accelerating structures. At X band, the dimensions are the same as the structure used in Figs. 3 and 4. At W band, we take $a=300\ \mu\text{m}$, $b=550\ \mu\text{m}$, $w=3500\ \mu\text{m}$, and $\epsilon_r=9.5$. Note that the parameters a , b , and ϵ_r are the same as the structure described in

Ref. [5]. The calculated results using our method differ slightly from Ref. [5] because the boundary conditions at $x = \pm w/2$ are different. We also analyzed the X -band structure using MAFIA code [11]. In Table I we only list the longitudinal propagation constant β and the quality factor Q of LSM_{11} synchronous mode. The analytical results agree well with computational results from MAFIA.

V. WAKEFIELD ANALYSIS

Normally, the wakefield calculation is tedious and cumbersome, and in this respect the rectangular structure is even more complicated than the cylindrical structure. However,

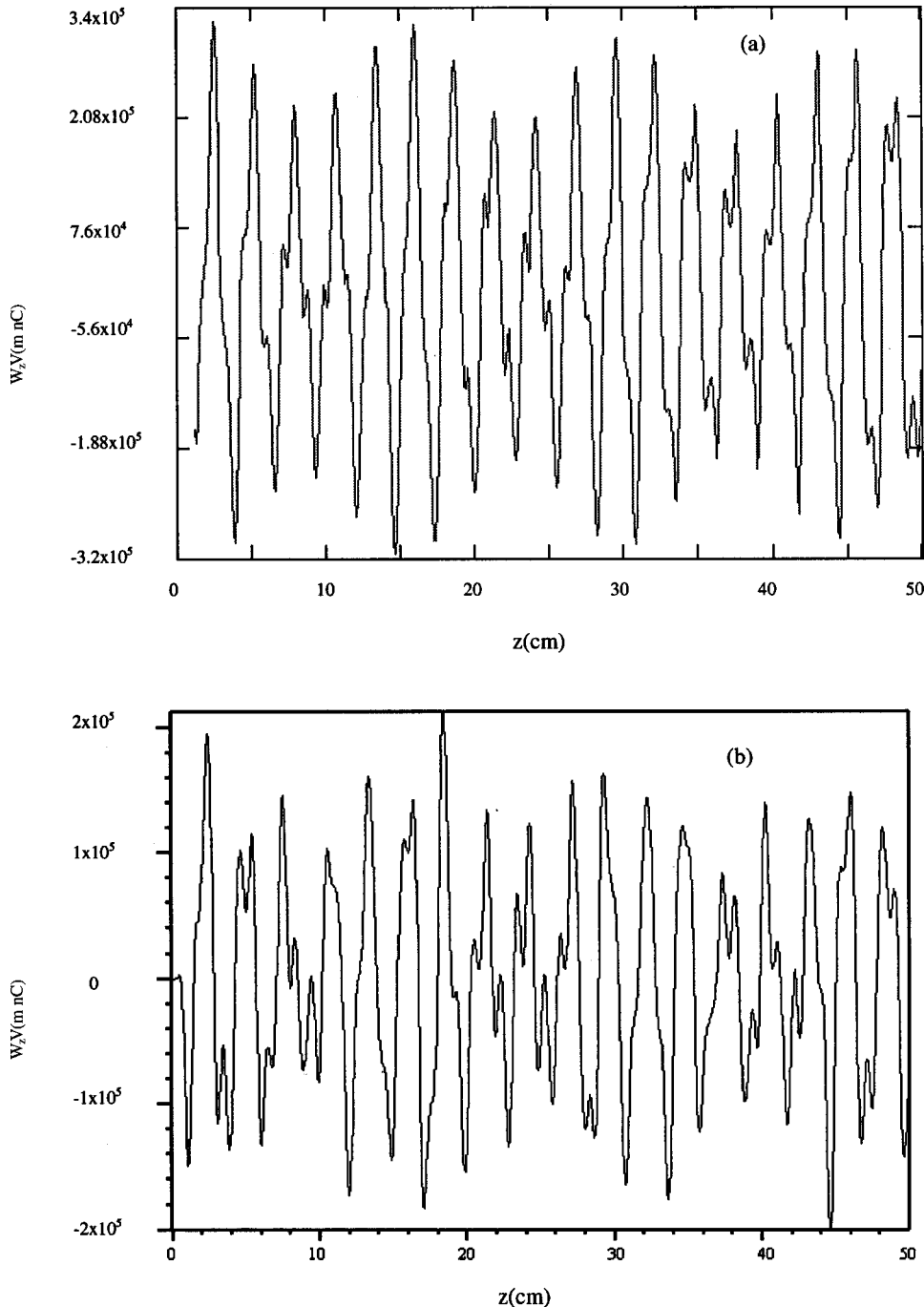


FIG. 6. Calculated longitudinal wakefield in an X -band structure using the field analysis method in Sec. II (a) and numerical results from MAFIA code (b). Results from (a) and (b) are in very good agreement ($a=3\ \text{mm}$, $b=5\ \text{mm}$, $w=23\ \text{mm}$, $\epsilon_r=10$, and $\sigma_z=2\ \text{mm}$, $q=1\ \text{nC}$).

since we have already obtained the field distribution and the normalized shunt impedance R/Q of each mode using mode analysis, the longitudinal component of the wakefield amplitude excited by a charged particle beam traveling on axis can be easily obtained as follows [12]:

$$E_{0i} = \frac{q\omega_i}{4} \left(\frac{R}{Q} \right)_i, \quad (20)$$

$$E_{zi} = E_{0i} \sin \frac{\pi}{w} \left(x + \frac{w}{2} \right) \cos k_{yi}^{(0)} y \cos \beta_i z, \quad (21)$$

where E_{0i} is the on-axis accelerating/decelerating gradient of the i th mode.

We assume a Gaussian longitudinal beam shape (with bunch length σ_z and charge q). The longitudinal wake $W_z(z)$ at distance z behind the drive electron beam is then given by

$$W_z(z) = \frac{1}{\sqrt{2\pi\sigma_z}} \int_{-\infty}^z \sum_{i=1}^{\infty} E_{0i} \cos \beta_i(z-z') \times \exp\left(-\frac{z'^2}{2\sigma_z^2}\right) dz'. \quad (22)$$

The transverse forces can be directly calculated from E_z by using the Panofsky-Wenzel theorem [13],

$$\frac{\partial \vec{F}_{\perp}}{\partial z} = e \nabla_{\perp} E_z,$$

$$\vec{F}_x(z) = \vec{x} \frac{e}{\sqrt{2\pi\sigma_z}} \int_{-\infty}^z \sum_{i=1}^{\infty} E_{0i} \frac{\pi}{w} \cos \frac{\pi}{w} \left(x + \frac{w}{2} \right) \times \cos k_{yi}^{(0)} y \cos \beta_i(z-z') \exp\left(-\frac{z'^2}{2\sigma_z^2}\right) dz', \quad (23a)$$

$$\vec{F}_y(z) = \vec{y} \frac{e}{\sqrt{2\pi\sigma_z}} \int_{-\infty}^z \sum_{i=1}^{\infty} E_{0i} (-k_{yi}^{(0)}) \times \sin \frac{\pi}{w} \left(x + \frac{w}{2} \right) \sin k_{yi}^{(0)} y \cos \beta_i(z-z') \times \exp\left(-\frac{z'^2}{2\sigma_z^2}\right) dz'. \quad (23b)$$

In Fig. 6(a), the longitudinal wakefields obtained using Eq. (19) are shown. For this example, a q is a 1nC bunch with length $\sigma_z = 2$ mm located at $z = 0$ moving along the axis with a speed of light in dielectric-loaded waveguide. The dielectric-loaded rectangular waveguide operated at X band has the same parameters described in Sec. III. The first five symmetric modes are used in the sum over modes; higher-order modes do not contribute significantly. We have compared our calculated results with those from direct numerical integration of the Maxwell equations using the MAFIA code.

VI. CONCLUSIONS

In this paper, we studied the dielectric-loaded rectangular waveguide accelerating structure. A detailed analytical field analysis method was presented. In this structure, an interesting phenomenon is that the two transverse wave numbers of the acceleration field in a synchronous acceleration mode are of equal amplitude and one is real and the other is imaginary. By using a beam line in which the accelerating structures are alternately rotated by 90° , the net acceleration energy gain experienced by a particle in a small central region can be made almost uniform. We also have analyzed the characteristic parameters and the longitudinal wakefield in a dielectric-loaded rectangular waveguide accelerating structure. Some results are presented and compared with numerical results from the MAFIA code and are found to be in good agreement.

Obviously, when the width of the structure tends to be very large, the dielectric-loaded rectangular waveguide accelerating structure can be thought of as a planar dielectric waveguide, and the effect of the metal walls at $x = \pm w/2$ should decrease. Pumping ports and tuning plungers can be located on the metal walls, then without significantly affecting the shape of the field. We are currently planning to fabricate and test experimentally the X band dielectric-loaded rectangular waveguide accelerating structure described above.

ACKNOWLEDGMENTS

We appreciate the help from Dr. Paul Schoessow throughout this work. This work is supported by Department of Energy, High Energy Physics Division, Advanced Technology Branch under Contract No. W-31-109-ENG-38.

[1] M. Rosing and W. Gai, Phys. Rev. D **42**, 1829 (1990).
 [2] King-Yuen Ng, Phys. Rev. D **42**, 1819 (1990).
 [3] S. Y. Park and J. L. Hirshfield, Phys. Rev. E **62**, 1266 (2000).
 [4] A. Tremaine, J. Rosenzweig, and P. Schoessow, Phys. Rev. E **56**, 7204 (1997).
 [5] Marc E. Hill, SLAC-R-560 (2000).
 [6] P. Zhou, W. Gai, R. Konecny, and X. Sun, Rev. Sci. Instrum. **71**, 2301 (2000).
 [7] J. W. Wang and G. A. Loew, SLAC-PUB-7684 (1997).
 [8] R. E. Collin, *Field Theory of Guided Waves*, 2nd ed. (Oxford University Press, New York, 1991).

[9] T. Itoh, *Numerical Techniques for Microwave and Millimeter-Wave Passive Structures* (Wiley, New York, 1989).
 [10] J. D. Jackson, *Classical Electrodynamics*, 2nd ed. (Wiley, New York, 1975).
 [11] MAFIA, Version 4.0 (Gesellschaft für Computer-Simulationstechnik, Lauteschlagstrabe 38, D-64289, Darmstadt, Germany).
 [12] H. H. Braun *et al.*, CERN-CLIC-Note 364, 1998.
 [13] W. K. H. Panofsky and W. A. Wenzel, Rev. Sci. Instrum. **27**, 967 (1956).